

Updated Collider Bounds on the Parameters of Dynamical Torsion

*Uma Mahanta*¹ and *Sreerup Raychaudhuri*²

¹Harish-Chandra Research Institute, Chhatnag Road, Allahabad 211019, India.

E-mail: mahanta@mri.ernet.in

²Department of Physics, Indian Institute of Technology, Kanpur 208016, India.

E-mail: sreerup@iitk.ac.in

ABSTRACT

We constrain the parameters of dynamical torsion, namely, the torsion-fermion coupling and the torsion mass, by making a careful analysis of current LEP-2 data at several energies, as well as CDF and D0 data from Run-I of the Tevatron. We find that measurements of the forward-backward asymmetry in the $e^+e^- \rightarrow \mu^+\mu^-$ channel at LEP-2 produce the most restrictive bounds over most of the parameter space, though other measurements, too, have a significant role to play. Our results considerably improve the existing constraints on models with dynamical torsion.

1 Introduction

The Standard Model (SM) has been extremely successful in explaining the results of all current experiments both at low and high energies. In spite of this phenomenal success, however, most high energy physicists think that the SM is at best an effective field theory valid at low energies — one of the main reasons being that the SM does not include quantum gravity. At the same time, many theorists believe that the ultimate fundamental theory will be provided some day by superstring theory since the low-energy effective Lagrangian of closed strings provides a finite theory of quantum gravity.

The low-energy effective action of closed strings predicts, along with a massless graviton, an antisymmetric second rank tensor $B_{\mu\nu}(x)$ – the Kalb-Ramond tensor – which enters the action via its antisymmetrised derivative $H_{\mu\nu\lambda} = \partial_{[\mu}B_{\nu\lambda]}$ [1]. The third rank tensor $H_{\mu\nu\lambda}$ is referred to as the torsion field strength. Torsion is thus a prediction of string theory. It is quite natural, therefore, to inquire what observable phenomena at low energies (e.g. collider effects) could be produced by the presence of torsion fields in the theory. From the point of view of string theory the interaction scale of torsion field should be related to and quite close to the string scale M_s . Traditionally one would expect this string scale to be of the order of the Planck mass $M_P \sim 10^{19}$ GeV, in which case it is extremely unlikely that laboratory observables would have any sensitivity to torsion effects. However Witten has shown [2] by explicit calculations in the strong-coupling regime using string duality that the string scale can be substantially lower than M_P . This result has been pushed to its extreme by Lykken[3] who speculated that the string scale could be as low as the electroweak scale – in which case torsion effects in laboratory experiments may be as strong as electroweak effects. Models of this kind make it particularly attractive to study the effects of dynamical torsion at the presently accessible collider energies of a few hundred GeV. In fact, it is keeping some such scenario in mind that the present study — a purely phenomenological one — has been carried out.

Some phenomenological effects at collider energies of heavy, non-propagating torsion fields have been considered in the literature[4]. The exchange of heavy torsion fields gives rise to dimension six four fermion interaction in the low-energy effective action. Non-propagating torsion therefore has only one unknown parameter namely the torsion interaction scale. Non-observation of deviations from the SM induced by these operators enables one to obtain a lower bound on the torsion scale Λ_{tor} . Dynamical and propagating torsion, on the other hand, has two unknown parameters, namely, the torsion mass (M_S) and the torsion coupling (η_S) to SM fields (fermions). The effects of dynamical torsion on precision measurements of forward-backward asymmetries at the CERN LEP-1 experiment, total cross-sections at LEP-1.5 and dilepton and dijet production at the Tevatron have been considered by Belyaev and Shapiro in Ref. [5] and bounds on the η_S – M_S plane have been obtained thereby. However, these

bounds are somewhat weak as a result of the low statistics available at the time their paper was written. Subsequently, both LEP-2 and the Fermilab Tevatron have acquired enormous amounts of data, all more-or-less confirming the SM predictions. It may be expected, therefore, that constraints on new physics beyond the SM will be more stringent than that before.

In this paper, therefore, we update the Belyaev-Shapiro bounds using the current LEP-2 data and published analyses of CDF and D0 data. In particular, we have used the LEP-2 analysis [7] at different energies for the forward-backward asymmetry A_{FB}^μ in the $\mu^+\mu^-$ channel and the data on total cross-section in $e^+e^- \rightarrow e^+e^-(\mu^+\mu^-)$. From the CDF Collaboration, we have used the dilepton Drell-Yan data $p\bar{p} \rightarrow e^+e^-(\mu^+\mu^-)$, and from D0, the dielectron data, to establish new, updated bounds on the torsion mass M_S and torsion fermion-coupling η_S . We find that, as expected, our results represent a considerable improvement over the earlier constraints. We demonstrate that the LEP-2 data on A_{FB}^μ produce the most restrictive bound over most of the parameter space. However, in the region of low torsion mass, where the torsion field can be resonantly produced at the Tevatron, the CDF and D0 data yield more stringent constraints.

2 The Torsion Lagrangian

The torsion tensor is defined in terms of the non-symmetric affine connection $\tilde{\Gamma}_{\beta\gamma}^\alpha$ by

$$T_{\beta\gamma}^\alpha = \tilde{\Gamma}_{\beta\gamma}^\alpha - \tilde{\Gamma}_{\gamma\beta}^\alpha. \quad (1)$$

This tensor clearly vanishes if the connection is symmetric in $\beta\gamma$, which is the case with, for example, conventional general relativity.

It is usually found convenient to divide the torsion tensor $T_{\beta\gamma}^\alpha$ into three irreducible components[5]. These are

(a) a *trace*: $T_\beta = \eta^{\alpha\gamma} T_{\alpha\beta\gamma}$;

(b) a *pseudo-trace*: $S^\delta = \epsilon^{\alpha\beta\gamma\delta} T_{\alpha\beta\gamma}$;

and (c) a third rank tensor $q_{\alpha\beta\gamma}$: which satisfies the conditions $q_{\beta\alpha}^\alpha = 0$ and $\epsilon^{\alpha\beta\gamma\delta} q_{\alpha\beta\gamma} = 0$.

It is clear that T_a behaves as a vector field and S_α as an axial vector field. However the simultaneous presence of both T_α and S_α , both of which are coupled to fermions in the low-energy effective Lagrangian, would lead, in the quantum theory, to serious problems arising from the $U(1)_A$ gauge anomaly. This problem may be circumvented in any one of two different ways. One way is to choose the couplings $\eta_T(f)$ and $\eta_S(f)$ of T and S respectively to a fermion pair $f\bar{f}$ so that $\sum_f C_f \eta_T^2(f) \eta_S(f) = 0$, where C_f is a color factor, in which case the $U(1)_A$ anomaly cancels. The other way — which we adopt in this paper — is to simply assume that the torsion tensor possesses a non-trivial pseudo-trace but *no* non-trivial trace. This is quite sensible from a phenomenological point of view. Moreover, such a situation does indeed arise if the torsion tensor is antisymmetric in all the three indices. We thus consider a

phenomenological scenario in which the vector field T_α is absent, while the axial vector field S_α interacts with fermions through an axial-vector coupling. In this case the relevant part of the Lagrangian can be written

$$\mathcal{L} = \mathcal{L}_{SM} - \frac{1}{4}S_{\mu\nu}S^{\mu\nu} + \frac{1}{2}M_S^2 S^\mu S_\mu + \sum_f \eta_S(f) \bar{\psi}_f \gamma_\mu \gamma_5 \psi_f S^\mu \quad (2)$$

where $S_{\mu\nu} = \partial_\mu S_\nu - \partial_\nu S_\mu$ and ψ_f represents a SM fermion (f) field. Note that the $U(1)_A$ gauge symmetry associated with the S field is softly broken by the fermion mass term contained in \mathcal{L}_{SM} and also by the torsion mass M_S . Further, in order that the $U(1)_A$ anomaly associated with $\gamma\text{--}\gamma\text{--}S$ and $Z\text{--}Z\text{--}S$ vertices should cancel, the axial charges of the SM fermions to the S field may be chosen [8] so that

$$\eta_S(u_i) = \eta_S(\nu_i) = -\eta_S(d_i) = -\eta_S(\ell_i) \equiv \eta_S^i \quad (3)$$

where u_i (d_i) correspond to quarks of charge $\frac{2}{3}$ ($-\frac{1}{3}$), and ℓ_i and ν_i correspond, respectively, to charged leptons and neutrinos belonging to the i^{th} generation. The above condition still allows the value of η_S^i to change from generation to generation, but in this paper we make the simplifying assumption that η_S^i is the same for all generations i.e. $\eta_S^i = \eta_S \forall i$. It is this generation-independent coupling constant η_S that we constrain using the recent LEP-2 and Tevatron data.

3 Torsion effects on LEP-2 and Tevatron observables

We have just seen that the pseudo-trace component of the torsion tensor effectively behaves as a massive spin-1 field with axial vector couplings to SM fermions. In many ways, therefore, its phenomenology is similar to that of an extra Z' -boson, and its presence will be manifest in the same kind of observables which are studied [9] in the context of Z' bosons. The main observables in question at an e^+e^- collider like LEP-2 are:

- The *total* cross-section for $e^+e^- \rightarrow f\bar{f}$, where f is any SM fermion. This will pick up extra contributions due to diagrams with S -field propagators and the interference of such diagrams with the SM diagrams. At LEP-2, data are available [7] for the $\mu^+\mu^-$, $\tau^+\tau^-$, Bhabha (e^+e^-) and dijet channels. While Bhabha scattering is an obvious first choice because of the large cross-section, data for the $\mu^+\mu^-$ channel are also clean and have small error-bars and can therefore be used very effectively. Data for the $\tau^+\tau^-$ and dijet channels are less useful because of the larger error-bars.
- The *differential* cross-section for $e^+e^- \rightarrow f\bar{f}$. It is well known that the presence of both vector and axial vector couplings in the effective Lagrangian would lead to parity violating signatures in collider experiments. The most convenient variable where it shows

up is the precision measurement of forward-backward asymmetry. A source of A_{FB}^f already exists in the SM because of the $\gamma_\mu\gamma_5$ component of Z and W -boson interactions with fermions. The presence of torsion with axial-vector type interactions will lead to additional parity-violating effects and change the forward-backward asymmetry from its SM value. It is not advisable to use the forward-backward asymmetry data for Bhabha scattering $e^+e^- \rightarrow e^+e^-$, because the large t -channel photon contribution creates a very large forward-backward asymmetry, which is highly sensitive to the angular cuts used in the analysis, and tends to overwhelm genuinely parity-violating effects.

An important possibility at LEP-2 is the fact that s -channel exchanges of the S -boson could lead to resonances in the total cross-section. For torsion masses accessible at LEP-2 energies, this would lead to enormous enhancements in the cross-section and the simple fact of their non-observance can be used to put stringent bounds on the torsion coupling η_S for the kinematically accessible region in the parameter space. However, virtual torsion fields can also contribute to LEP-2 observables. As the measured values of almost all observables at LEP-2 are known to be in excellent agreement with their SM predictions, it follows that one can establish bounds on torsion parameters over their entire range, subject only to the limitations imposed by experimental errors.

The situation at the Tevatron is generally similar, but with some important differences. We can look for torsion contributions to $q\bar{q} \rightarrow f\bar{f}$, where the observable final state would have dileptons or dijets. However, it is not feasible to study dijets because the enormous QCD background would tend to swamp any torsion effects. We, therefore, limit our study to Drell-Yan dileptons only, and, in particular, to (a) the CDF data [10] on $p\bar{p} \rightarrow e^+e^-(\mu^+\mu^-)$ and (b) the D0 data [11] on $p\bar{p} \rightarrow e^+e^-$. In every case, the S -boson contribution arises through an s -channel propagator, as in the case of $e^+e^- \rightarrow q\bar{q}$. Since the energy of the initial-state partons is variable, some of the events are always sure to hit an S -resonance, should it be kinematically accessible. This leads to large torsion contributions, and hence — since the observed data match the SM predictions very well — to strong constraints. As the torsion mass M_S increases, the Bjorken variables x_1, x_2 required for resonant production go up and the consequent steep fall in parton luminosities kills the cross-section, thereby weakening the constraints. In each case, we have considered the bin-wise invariant mass distribution only. The CDF Collaboration has also presented [10] forward-backward asymmetry measurements in $p\bar{p} \rightarrow e^+e^-$, but these data have large errors which are traceable to the low charge-identification efficiencies for e^\pm . Hence, we have elected not to use this data for our analysis. The D0 Collaboration has presented the invariant mass distribution for dielectrons, but were unable to make forward-backward asymmetry measurements since their detector lacks a central magnetic field [11]. Thus, a similar analysis is required for all three sets of experimental data from the Tevatron.

4 Torsion constraints from LEP-2 data

In this paper we have focused on the following measurements:

1. The total cross-section $\sigma(e^+e^- \rightarrow \mu^+\mu^-)$, which is compared with the SM value σ_{SM} by studying the ratio σ/σ_{SM} .
2. The forward-backward asymmetry in the muon channel A_{FB}^μ , which is compared with the SM value $A_{FB}^{\mu(SM)}$ by studying the difference $A_{FB}^\mu - A_{FB}^{\mu(SM)}$.
3. The total cross-section $\sigma(e^+e^- \rightarrow e^+e^-)$ for Bhabha scattering.

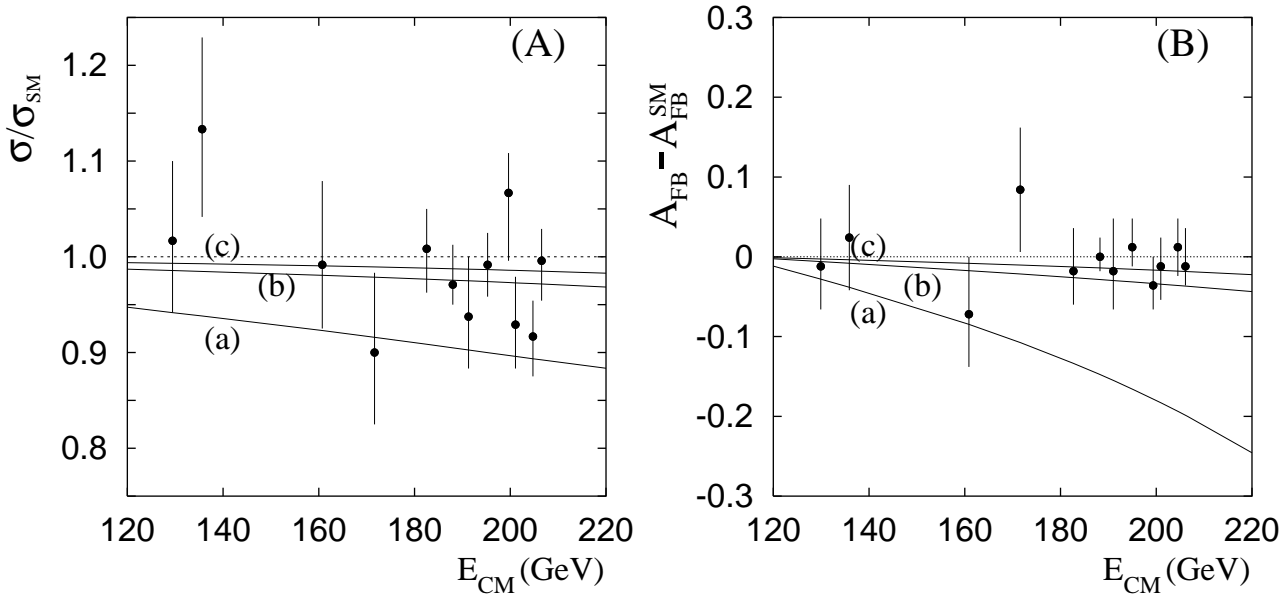


Figure 1: Illustrating the torsion contributions to the process $e^+e^- \rightarrow \mu^+\mu^-$ at LEP-2. We plot (A) the ratio σ/σ_{SM} and (B) the difference $A_{FB}^\mu - A_{FB}^{\mu(SM)}$. The dotted line represents the SM prediction; solid lines represent the torsion effects for (a) $M_S = 500$ GeV; $\eta_S = 0.3$, (b) $M_S = 1$ TeV; $\eta_S = 0.3$, and (c) $M_S = 500$ GeV; $\eta_S = 0.1$. The points with error-bars represent data from LEP-2.

The exact form in which these variables are taken is determined by the experimental data presented [7] by the LEP-2 Collaborations at DPF-2002. The use of σ/σ_{SM} is well-known to cancel out the principal effects due to initial state radiation. The use of $A_{FB}^\mu - A_{FB}^{\mu(SM)}$ isolates the new physics contribution to forward-backward asymmetry. In Figure 1 we present a comparison of torsion effects with the SM prediction and the LEP-2 data for (A) σ/σ_{SM} and (B) $A_{FB}^\mu - A_{FB}^{\mu(SM)}$ respectively. The dotted line represents the SM predictions (1 and 0 respectively), while solid lines represent the results of including torsion effects for

(a) $M_S = 500$ GeV; $\eta_S = 0.3$,

(b) $M_S = 1$ TeV; $\eta_S = 0.3$,

and (c) $M_S = 500$ GeV; $\eta_S = 0.1$.

The points with error-bars represent data from LEP-2 at different energies. It is immediately clear that the data are usually within 1σ of the SM value. It is also clear that substantial deviations from the SM prediction occur only if the torsion mass is relatively light and the torsion-fermion coupling is close to electroweak strength. Even then, the total cross-section shows a relatively small deviation; for the forward-backward asymmetry, however, for energies above around 180 GeV, the deviation can be considerable. It follows that we can derive a strong bound using the $A_{FB}^\mu - A_{FB}^{\mu(SM)}$ data. In order to do this, the general procedure adopted has been to calculate a χ^2 for the data on a variable Q using the formula

$$\chi^2(\eta_S, M_S) = \sum_i \frac{[Q_i^{th}(\eta_S, M_S) - Q_i^{c.v.}]^2}{(\delta Q_i^{exp})^2} \quad (4)$$

where i runs over the different values of E_{CM} at LEP-2, $Q_i^{th}(\eta_S, M_S)$ is the theoretically-computed value, $Q_i^{c.v.}$ is the experimental central value and δQ_i^{exp} represents the experimental error. As the errors presented by the LEP-2 collaborations are asymmetric, we choose the error-bar on the same side of the central value as the theoretical curve. Constraints may now be obtained by varying η_S, M_S and demanding that the resultant χ^2 should not exceed the value permissible for random Gaussian variables. This has, in fact been done in Figure 2, where we constrain the η_S - M_S plane using these two measurements. It is obvious from Figure 2 that the forward-backward asymmetry measurement is the more useful one in constraining torsion parameters. We attribute this to the fact that the A_{FB}^μ parameter is not affected by the large QED contribution.

We now turn to Bhabha scattering, which is a somewhat more complicated calculation, given the fact that there are t as well as s -channel contributions from photon, Z -boson and S -boson propagators, with interference terms between all the contributions [12]. Figure 3(A) shows the excess contributions compared with the SM (dotted line) as solid lines for

$$(a) \ M_S = 300 \text{ GeV}; \ \eta_S = 0.3,$$

$$(b) \ M_S = 500 \text{ GeV}; \ \eta_S = 0.3,$$

$$\text{and } (c) \ M_S = 800 \text{ GeV}; \ \eta_S = 0.3,$$

where, the points with error-bars represent, as before, data from LEP-2 at different energies [7]. Clearly, one obtains substantial deviations only for lighter values of M_S . Making a χ^2 analysis as before, we obtain constraints on the parameter space illustrated in Figure 3(B). Because of the small error-bars in Bhabha scattering data, the constraints arising from this rival those from the forward-backward asymmetry, at least up to about $M_S \approx 1.7$ TeV, after which the Bhabha scattering process shows little or no contribution from S -bosons.

If we compare these bounds with those obtained earlier [5] using LEP-1.5 data, we notice an enormous improvement, which is primarily due to the fact that the error-bars decrease at higher LEP energies: a result of the higher luminosity accumulated at these energies. The

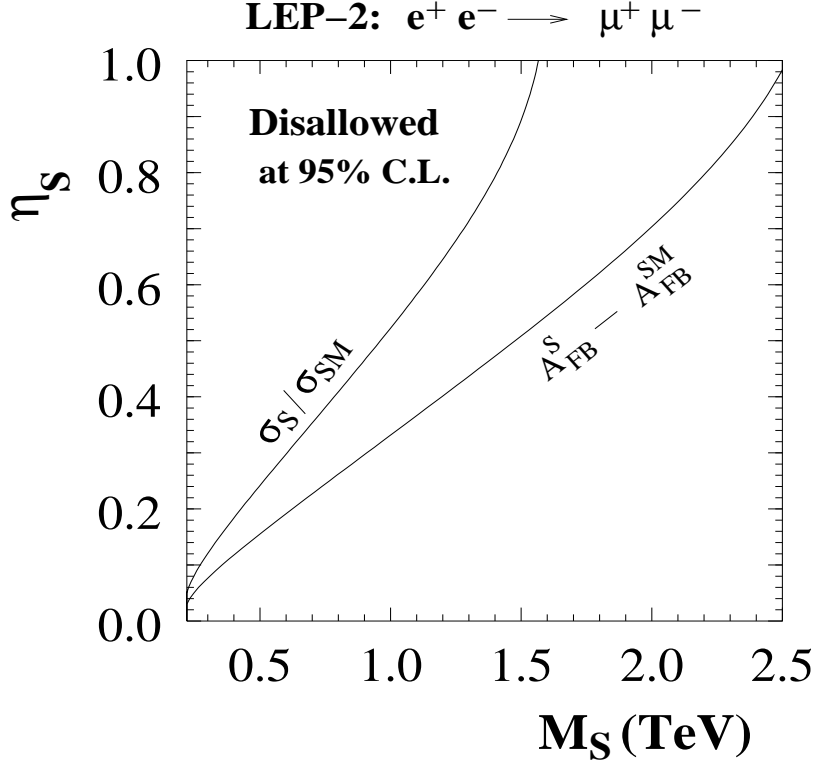


Figure 2: Illustrating LEP-2 constraints on the parameter space obtained from data on $e^+e^- \rightarrow \mu^+\mu^-$.

smaller error-bars are most significant in Figure 3(A). In any case, it may be argued that the higher the energy, the closer we are to a heavy S -resonance and the larger must be the corresponding torsion contribution. Hence we should expect even more stringent bounds at a 500 GeV or 1 TeV linear e^+e^- collider or, perhaps, at a high energy muon collider where center-of-mass energies as high as 3–4 TeV or even as high as 10 TeV have been contemplated [13].

5 Torsion constraints from Tevatron data

At the Tevatron collider, running (Run-I) at a center-of-mass energy of 1.8 TeV, we would expect to see torsion resonances in $p\bar{p} \rightarrow e^+e^-(\mu^+\mu^-)$, as explained earlier. The best observables where this would show up would be in the bin-wise invariant mass distribution given, for example, by both CDF and D0 Collaborations, where a distinct peak would appear at the mass of the resonance. We have calculated the parton-level cross-sections keeping in mind different signs for the S -boson couplings to u and d quarks, according to the convention of Eqn. 3. The CDF and D0 data are reproduced in Table 1. For our numerical analysis of the CDF e^+e^- data, the parton-level cross-section with torsion effects included is incorporated into a Monte Carlo event generator, running subject to the following kinematic cuts:

- The final state electron (positron) should have pseudorapidity within $|\eta_e| < 4.2$ to be detected in the electromagnetic calorimeter. The pseudorapidity coverages in the CDF

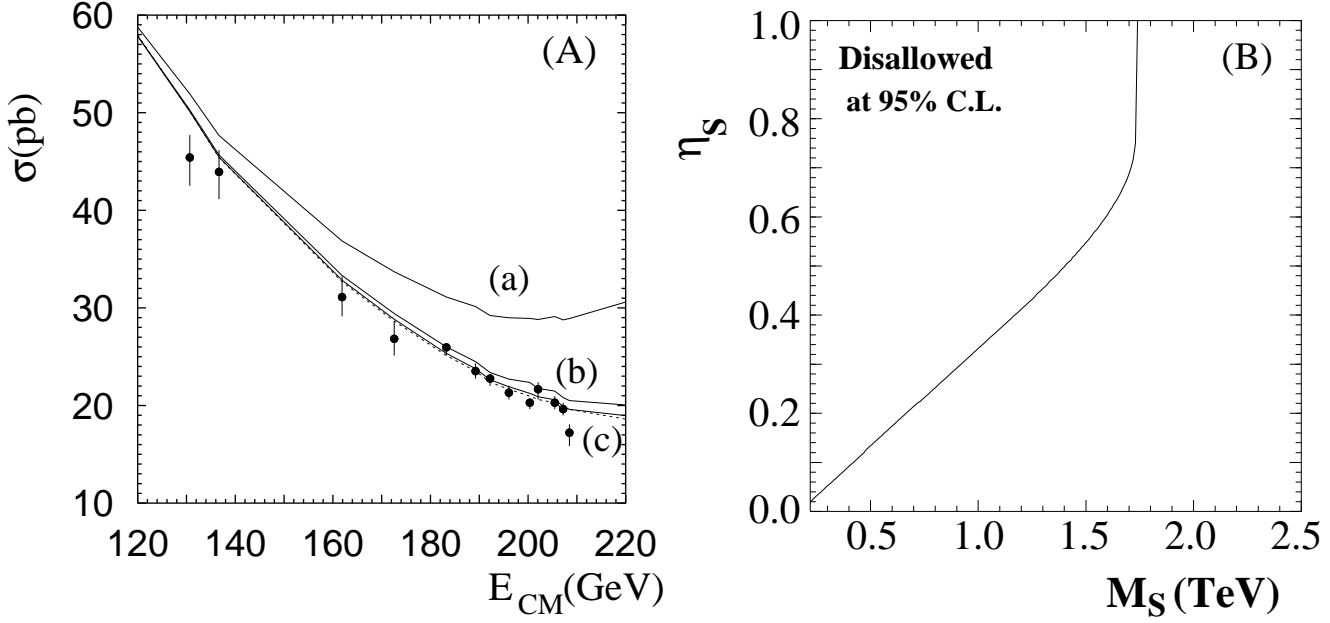


Figure 3: Illustrating the torsion contributions to the Bhabha scattering process $e^+e^- \rightarrow e^+e^-$ at LEP-2. (A) shows the cross-section: the dotted line represents the SM prediction, solid lines represent the torsion effects for (a) $M_S = 300$ GeV; $\eta_S = 0.3$, (b) $M_S = 500$ GeV; $\eta_S = 0.3$, and (c) $M_S = 800$ GeV; $\eta_S = 0.3$, while the points with error-bars represent data from LEP-2. The corresponding 95% C.L. constraints on the parameter space are shown in (B).

detector are: $|\eta_e| < 1.1$ for the central calorimeter, $1.1 < |\eta_e| < 2.4$ for the end plug, and $2.2 < |\eta_e| < 4.2$ for the forward calorimeter.

- At least one final state electron (positron) should have pseudorapidity $|\eta_e| < 2.4$ so that it does not lie in the forward calorimeter.
- The minimum transverse momentum p_{T_e} of the electron (positron) should be 22, 20 or 15 GeV, depending on whether it passes into the central calorimeter, end cap or forward calorimeter.
- The electron (positron) tracks should not be back-to-back. This reduces the cosmic ray background. To implement this we demand that the dielectron opening angle should satisfy $\theta_{ee} < 175^\circ$.

These kinematic cuts are identical with the ones used by the CDF Collaboration in their analysis [10], so far as they can be translated to a parton-level analysis. Our numerical results compare well with the experimental numbers given in the first part of Table 1.

For a dimuon final state, the kinematic cuts are much simpler. We demand

- The final state muons should have pseudorapidity $|e_\mu| < 1.1$, which is the coverage of the muon chambers.

- The final state muons should have a minimum transverse momentum $p_{T\mu} > 2.8$ GeV, which is required for triggering.
- The dimuon opening angle should satisfy $\theta_{\mu\mu} < 175^\circ$, to eliminate cosmic ray backgrounds.

| CDF | e^+e^- | | | | | | | | |
|---------------------|----------------------|----------------------|----------------------|----------------------|----------------------|----------------------|----------------------|----------------------|----------------------|
| $M_{e^+e^-}$ | 105–120 | 120–140 | 140–200 | 200–300 | 300–400 | 400–600 | 600–999 | | |
| σ (pb) | 3.934 | 1.309 | 1.249 | 0.260 | 0.081 | 0.028 | 0.000 | | |
| $\delta\sigma$ (pb) | ± 0.355 | ± 0.203 | ± 0.192 | ± 0.085 | ± 0.047 | ± 0.028 | ± 0.036 | | |
| CDF | $\mu^+\mu^-$ | | | | | | | | |
| $M_{\mu^+\mu^-}$ | 110–120 | 120–150 | 150–200 | 200–300 | 300–400 | 400–600 | 600–999 | | |
| σ (pb) | 2.319 | 2.418 | 0.699 | 0.391 | 0.056 | 0.000 | 0.000 | | |
| $\delta\sigma$ (pb) | ± 0.516 | ± 0.478 | ± 0.233 | ± 0.158 | ± 0.056 | ± 0.040 | ± 0.044 | | |
| D0 | e^+e^- | | | | | | | | |
| $M_{e^+e^-}$ | 120–160 | 160–200 | 200–240 | 240–290 | 290–340 | 340–400 | 400–500 | 500–600 | 600–1000 |
| σ (pb) | 1.930 | 0.490 | 0.280 | 0.066 | 0.033 | 0.057 | 0.039 | 0.037 | 0.035 |
| $\delta\sigma$ (pb) | $+0.430$ -0.440 | $+0.160$ -0.180 | $+0.090$ -0.100 | $+0.052$ -0.058 | $+0.032$ -0.030 | $+0.042$ -0.047 | $+0.024$ -0.039 | $+0.023$ -0.037 | $+0.023$ -0.035 |

Table 1: *Drell-Yan data from the Tevatron showing the observed cross-section with error-bars deposited in different bins of dilepton invariant mass. The CDF and D0 data are taken from Refs. [10] and Ref. [11] respectively. All invariant masses are measured in GeV.*

With these cuts our numbers agree well with the second part of Table 1. For parton fluxes we have followed the CDF Collaboration in using the MRST99 structure functions [14], and we have also incorporated next-to-leading-order QCD corrections in the same way as the CDF Collaboration have, namely, by weighting the events with a K -factor [15]

$$K(\hat{s}) = 1 + \frac{4}{3} \left(1 + \frac{4}{3} \pi^2 \right) \frac{\alpha_s(\hat{s})}{2\pi} . \quad (5)$$

The D0 Collaboration has presented [11] a similar set of e^+e^- data, as shown in the last part of Table 1. To compare our predictions with their data, we use the following set of kinematic cuts.

- The final state electron (positron) must lie within the angular coverage of the electromagnetic calorimeter, i.e. it must have either $|\eta_e| < 1.1$ to be in the central calorimeter (CC) or $1.5 < |\eta_e| < 2.5$ to be in the forward calorimeters (EC).
- The final state electron (positron) must have a minimum transverse energy $E_{Te} > 20$ GeV.
- The dielectron opening angle should satisfy $\theta_{ee} < 175^\circ$ in order to eliminate cosmic ray backgrounds.

QCD corrections are included by the inclusion of a K -factor. Following the D0 Collaboration, we make a numerical calculation of the K -factor by comparing our LO results for the SM cross-section with the NNLO calculations of Ref. [16]. We have used MRS(A') structure functions [17], again following the D0 Collaboration. With these included, our cross-sections match well with the D0 data given in the last part of Table 1.

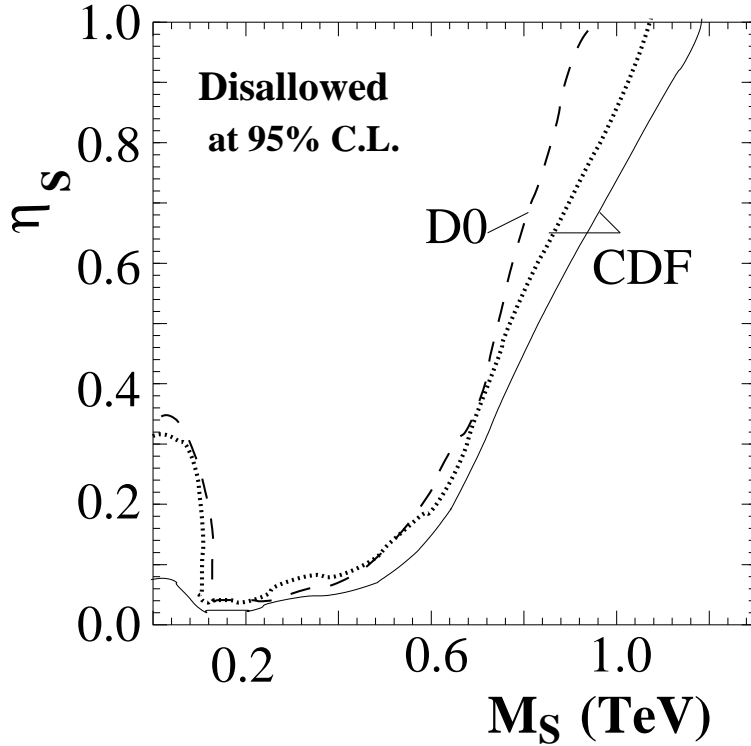


Figure 4: 95% C.L. constraints on the parameter space obtained from Drell-Yan data measured in Run-I of the Tevatron. The solid (dotted) curve corresponds to dielectron (dimuon) final states at the CDF detector, while the dashed curve corresponds to dielectron final states at the D0 detector.

Using the above tools, we are now in a position to generate the invariant mass distribution for the torsion-inclusive theory and compare it with the CDF and D0 data. Since we are handicapped by not knowing the actual value of the torsion mass, it is sensible to make a χ^2 analysis of the invariant mass distribution using the same formula as in Eqn. (4), except that the sum now runs over invariant mass bins rather than E_{CM} values. Once again, requiring that the calculated χ^2 for a given pair of (η_S, M_S) should not exceed the maximum value permissible for random Gaussian fluctuations, we obtain constraints on the η_S – M_S plane. Clearly, the presence of a resonance would send the χ^2 shooting up; on the other hand, the result will be somewhat diluted by the inclusion of the other mass bins, where the deviation will be minimal. Accepting these features of the statistical method, we present our results in Figure 4. It is clear that torsion masses up to about 600 GeV are very strongly constrained by the Drell-Yan data; beyond this, as has been explained, the rapid fall in parton fluxes weakens

the bound considerably, so that, in fact, it is no longer competitive with LEP-2 bounds.

It is also clear that the CDF dielectron data provide marginally stronger constraints on torsion parameters than the CDF dimuon and D0 dielectron data. The first is not unexpected, as the CDF dielectron data have smaller error-bars than the dimuon data. On the other hand, the D0 dielectron data, though having comparable error-bars, yield a slightly poorer constraint. We attribute this to the marginally larger number of bins (9 instead of 7), which creates a greater dilution effect in our χ^2 analysis, as explained above. The difference between the solid and dashed curves in Figure 4 is, therefore, primarily an artifact of our somewhat naive statistical method. As all the three data sets produce results in the same ballpark, however, we do not consider it worthwhile, at the present stage, to try a more sophisticated statistical method [18] for the D0 constraints. Moreover, we shall show in the next section that in the region where the three curves differ, a stronger constraint is provided anyway by the LEP-2 data analyzed in the previous section.

6 Combined bounds

In Figure 5, we have shown the constraints on the η_S – M_S plane by combining the most significant of the constraints obtained above. These are the following:

- (a) constraint from σ/σ_{SM} for $e^+e^- \rightarrow \mu^+\mu^-$ at LEP-2;
- (b) constraint from $A_{FB}^\mu - A_{FB}^{\mu(SM)}$ at LEP-2;
- (c) constraint from Bhabha scattering at LEP-2;
- (d) constraint from $p\bar{p} \rightarrow e^+e^-$ at the Tevatron (CDF).

Obviously, constraint (b) is the most effective of the LEP-2 constraints, except for a tiny sliver of parameter space between 600–850 GeV, where Bhabha scattering is marginally more restrictive. Below 600 GeV, however, the strongest constraints come from the CDF dielectron data (d). We have not included the CDF dimuon data or the D0 dielectron data because the CDF dielectron data turn out to be more effective in constraining the torsion parameters.

Taken all together, we rule out a considerable area in the parameter space (roughly double the area ruled out in the earlier analyses). Among other things, it is clear that if the torsion coupling is to be of electroweak strength ($\eta_S \sim 0.3 - 0.6$), then the torsion mass will be pushed up well above a TeV. If, on the other hand, the torsion-fermion coupling is weak ($\eta_S \sim 0.01$), there is practically no laboratory bound and it would still be possible to have very light excitations of the torsion field.

At Run-II of the Tevatron, which is currently in progress, we expect some improvement in the bounds because of two circumstances. In the first place, the center-of-mass energy is marginally higher (2 TeV) and hence the kinematic reach for resonant S -bosons also increases marginally. Within this region, the accumulation of high luminosity could strengthen the

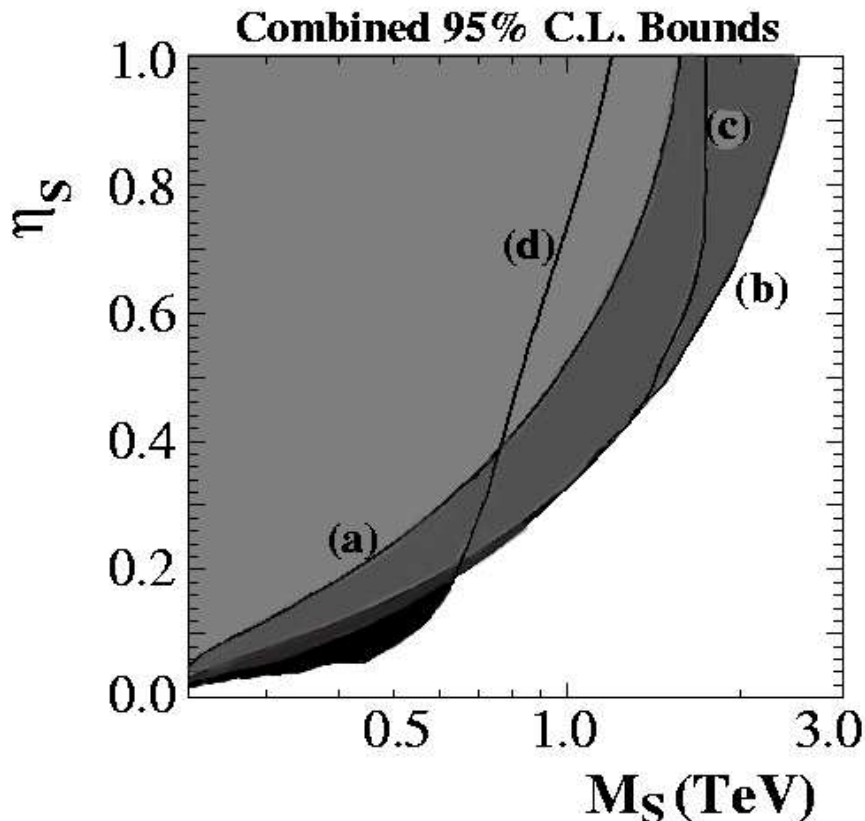


Figure 5: Combined constraints on the parameter space obtained from LEP-2 and the Tevatron. These 95% C.L. curves correspond to (a) σ/σ_{SM} and (b) $A_{FB}^\mu - A_{FB}^{\mu(SM)}$ for $e^+e^- \rightarrow \mu^+\mu^-$ at LEP-2; (c) Bhabha scattering at LEP-2; (d) the CDF measurement of $p\bar{p} \rightarrow e^+e^-$ at the Tevatron.

constraint on the coupling η_S . This would also better the present bound on η_S in the non-resonant region, but not, perhaps, very significantly. It is unlikely, therefore, that Run-II constraints would be competitive with LEP-2 results when the torsion mass is of the order of a TeV or more.

7 Discussion and Conclusions

Before we conclude, we need to take note of some important points. We have assumed that the coupling η_S is universal, i.e. the same for every generation. If this assumption is relaxed, the constraints from Bhabha scattering and from Drell-Yan dielectrons become constraints on the first generation coupling η_{S1} , while those from $e^+e^- \rightarrow \mu^+\mu^-$ and from Drell-Yan dimuons become constraints on the combination $\sqrt{\eta_{S1}\eta_{S2}}$. Combining the two could yield constraints on η_{S2} alone. In a similar way, we could derive (weaker) constraints on η_{S3} by using the LEP-2 data on $e^+e^- \rightarrow \tau^+\tau^-$. However, such an exercise would become worthwhile only if there is some *empirical* reason to suspect that the torsion couplings could change from generation to generation.

In our analysis of collider bounds, we have focused on the effects of light dynamical torsion

with weak coupling $\eta_S \leq 0.1 - 1.0$ to fermions. Our results, as shown in Figure 5, demonstrate that with increasing η_S , the lower bound on M_S is driven to higher values. It follows that for strong torsion-fermion couplings (e.g. $\eta_S \simeq \sqrt{4\pi}$) the results obtained with high mass dynamical torsion would more-or-less agree with those of non-propagating torsion, which are already available in the literature [4].

In this paper we have considered the collider effects of the pseudo-trace component S_μ of the torsion tensor only and assumed that the trace field T_μ vanishes. However it is also possible to consider a scenario in which the torsion tensor is symmetric in any two indices. In this scenario S_μ vanishes but T_μ has a non-trivial value. Since S_μ is an axial vector but T_μ is a vector, the forward-backward asymmetry that they produce are expected to differ significantly. In the case of S_μ the additional A_{FB} due to torsion arises from the photon- S_μ interference and the interference between S_μ and the vector coupling of Z_μ . However since the vector coupling of Z_μ to charged leptons is very small the later contribution is expected to be small except near the Z -pole or S -pole. On the other hand in the case of T_μ the additional contribution to A_{FB} arises from the interference between T_μ and the axial vector coupling of Z_μ . Since the axial coupling of Z_μ to charged leptons is quite large, the later contribution is expected to be appreciable even away from Z and S -boson pole. The bounds in the $\eta_S - M_S$ plane arising from current collider data are therefore expected to differ from the case of S_μ .

To sum up, then, we have updated the collider bounds on dynamical torsion in a scenario where only the pseudo-trace field S_μ couples to fermions, with a universal coupling. Using current data from LEP-2 and the Tevatron, we find that torsion fields up to about 600 GeV are excluded unless the torsion-fermion coupling drops below 0.1. This is a much stronger constraint than those obtained from considering either the anomalous magnetic moment of the muon [19] or the earlier LEP1, LEP-1.5 and Tevatron data. As more data is accumulated at Run-II of the Tevatron, we expect this bound to improve, but this improvement may be only marginal, as Tevatron constraints are severely limited by the kinematic reach of the machine. The commissioning of high-energy machines like the CERN LHC and a possible linear e^+e^- collider would increase the discovery reach for torsion fields enormously. A really high energy machine, like, for example, a muon collider running at 3–4 TeV center-of-mass energy, would be enormously effective in such searches. Till such data are available, however, we expect our results to more-or-less represent the state-of-the-art for laboratory constraints on dynamical torsion scenarios.

Acknowledgments

The authors acknowledge useful discussions with S. Banerjee. SR would like to further thank N.K. Mondal and S.K. Rai for discussions. UM thanks the Department of Physics, Indian Institute of Technology, Kanpur for hospitality; SR likewise extends thanks to the Harish-Chandra Research Institute, Allahabad.

References

- [1] M.B. Green, J.H. Schwarz and E. Witten, *Superstring Theory*, Cambridge University Press, Cambridge, 1987;
M. Kalb and P. Ramond, *Phys. Rev.* **D9**, 2273 (1974);
P.K. Townsend, *Phys. Lett.* **B88**, 97 (1979);
R. Hammond, *Rep. Prog. Phys.* **65**, 599 (2002);
I.L. Shapiro, *Phys. Rept.* **357**, 113 (2001).
- [2] E. Witten, *Nucl. Phys.* **B471**, 135 (1996).
- [3] J. Lykken, *Phys. Rev.* **D54**, 3693 (1996).
- [4] V. Barger, K. Cheung, K. Hagiwara and D. Zeppenfeld, *Phys. Rev.* **D57**, 391 (1998).
- [5] A.S.Belyaev and I.L. Shapiro, *Phys. Lett.* **B425**, 246 (1998); *Nucl. Phys.* **B543**, 20 (1999).
- [6] I.L. Buchbinder, S.D. Odintsov and I.L. Shapiro, *Effective Action in Quantum Gravity*, IOP Publishing–Bristol (1992);
F.W. Hehl, P. Von Der Heyde, G.D. Kerlick and J.M. Nester, *Rev. Mod. Phys.* **48**, 393 (1976).
- [7] M.W. Gr newald, *Nucl. Phys. Proc. Suppl.* **117**, 280 (2003).
- [8] We make no attempt, in this work, to motivate such a choice, which is clearly not unique. We could, for example, have chosen opposite signs for all the couplings. We have checked that making that choice would lead to somewhat less restrictive constraints from Tevatron data. LEP-2 constraints would, of course, remain unaffected.
- [9] J.L. Hewett and T.G. Rizzo, *Phys. Rept.* **183**, 193 (1989).
- [10] CDF Collaboration, T. Affolder *et al*, *Phys. Rev. Lett.* **87**, 131802 (2001).
- [11] D0 collaboration, B. Abbott *et al*, *Phys. Rev. Lett.* **82**, 4769 (1999).
- [12] V. Barger and R.J.N. Phillips, *Collider Physics*, Addison-Wesley (1987).
- [13] See, for example, M.S. Berger, Proc. of *Montauk 1999, Colliders and collider physics at the highest energies*, p.32, hep-ph/0001018 (2000).
- [14] A.D. Martin *et al*, *Eur. Phys. J.* **C14**, 133 (2000).
- [15] G. Altarelli, R.K. Ellis and G. Martinelli, *Nucl. Phys.* **B157**, 461 (1979).
- [16] R. Hamberg, W.L. van Neerven and T. Matsuura, *Nucl. Phys.* **B359**, 343 (1991).

- [17] A.D. Martin, R.G. Roberts and W.J. Stirling, *Phys. Rev.* **D50**, 6734 (1994); *ibid.* **D51**, 4756 (1995).
- [18] Such as, for example, the use of Bayesian statistics, which are relevant when a few events are seen and are now employed by the D0 Collaboration as a matter of course.
- [19] P. Das, U. Mahanta and S. Raychaudhuri, hep-ph/0211137.